RSC Advances

PAPER

View Article Online
View Journal | View Issue

Cite this: *RSC Adv.*, 2015, **5**, 101656

Growth of branched gold nanoparticles on solid surfaces and their use as surface-enhanced Raman scattering substrates†

N. I. Evcimen,[a] S. Coskun,[b] D. Kozanoglu,[c] G. Ertas,[a] H. E. Unalan[bc] and E. Nalbant Esenturk*[ac]

Received 10th September 2015
Accepted 18th November 2015

DOI: 10.1039/c5ra18570j

www.rsc.org/advances

Branched gold (Au) nanoparticles (NPs) were synthesized directly on surfaces of three different supports (silicon, glass, indium tin oxide (ITO)) by following a "seed-mediated" method. Growth of the nanostructures in high yield and all with branched morphology was achieved on all surfaces. Nanostructures with desired characteristics were synthesized by determining the optimum seed size (8 nm Au nanospheres) and pH (3.00) of the growth solution. The Au NPs synthesized under these conditions have branched morphologies with average sizes of *ca.* 450 nm and are well dispersed on the support surface. Surface-enhanced Raman scattering (SERS) spectroscopy studies were performed using Rhodamine 6G (R6G) as a probe molecule. The results revealed strong SERS activity of the synthesized Au NPs for the detection of R6G in concentrations as low as 1 nM with an enhancement factor (EF) estimated as greater than 8 orders of magnitude.

1. Introduction

The synthesis, functionalization and utilization of nanoparticles (NPs) have become a focus of intense research. This well-deserved attention is mostly due to their very special optical properties that can be manipulated with the control of NP size and shape. In particular, Au NPs with sharp features produce strong electric fields at the tips or edges of NPs upon absorption of incident light in the visible and/or near IR region.[1–6] They also show very high sensitivity to changes in their dielectric environment.[1–3] All these make Au NPs very attractive for applications requiring special optical properties, such as photovoltaic devices, sensors, electronic and biomedical applications.[6–14]

NPs should be stabilized on planar solid surfaces for their further utilization in almost all of these aforementioned applications. One way to achieve this is using sophisticated lithographical methods.[15] Another way is to immobilize synthesized nanostructures on substrates with covalent interactions to form monolayers.[16] Growing nanostructures directly on surfaces with various deposition techniques (*i.e.* electrochemical, physical and chemical vapor deposition) or solution based methods (*i.e.* "seed-mediated" growth) have also been reported.[17–19] Among all these methods, the "seed-mediated" growth described by Murphy and co-workers has some advantages over the other ones. For instance, it provides an access to prepare Au NPs with different sizes and shapes in aqueous media.[20–24] In addition, control over NP morphology and yield by manipulating parameters such as the reactant concentration, seed characteristics and pH of the reaction media make this approach very attractive.[25] The method has been used to synthesize numerous anisotropic Au NPs in aqueous solutions for over a decade.[20–22] More recently, this method has also been utilized to grow Au NPs directly on planar surfaces.[19,26] In particular, Au NPs with spherical and rod like morphologies have been synthesized on different substrates such as ITO, mica and glass with seed mediated approach.[19,26] As it was reported in the literature, branched, spiky and star shaped Au NPs demonstrate strong SERS activities in the detection of the molecules.[1–6] However, to the best of our knowledge, these nanostructures with superior optical properties have not been synthesized directly on surfaces, yet.

In this study, branched Au NPs were synthesized on Si, ITO and glass substrates by using "seed-mediated" growth. The important process parameters such as pH of the growth solution and seed characteristics were optimized to synthesize the nanostructures in high yield and all with branched morphologies. In addition, SERS activity of these Au NPs on substrates was then demonstrated for their further sensing applications.

[a]*Department of Chemistry, Middle East Technical University (METU), 06800 Ankara, Turkey. E-mail: emren@metu.edu.tr*

[b]*Department of Metallurgical and Materials Engineering, METU, 06800 Ankara, Turkey*

[c]*Micro and Nanotechnology Program, METU, 06800 Ankara, Turkey*

† Electronic supplementary information (ESI) available. See DOI: 10.1039/c5ra18570j

2. Experimental procedures

2.1. Materials

L-Ascorbic acid (AA), silver nitrate ($AgNO_3$), hydrogen tetrachloroaurate(III) trihydrate ($HAuCl_4 \cdot 3H_2O$), sodium hydroxide (NaOH), (3-aminopropyl)-trimethoxysilane (APTMS) and toluene were purchased from Sigma-Aldrich; trisodium citrate dihydrate, sodium borohydride ($NaBH_4$), sulfuric acid (H_2SO_4) and hydrochloric acid (HCl) were purchased from Merck; cetyltrimethylammonium bromide (CTAB) and Rhodamine 6G (R6G) were purchased from Fluka and used without further purification. ITO film-coated glass was purchased from Delta Technologies (20 Ω, size *ca* 7 × 50 × 0.7 mm). Si-wafer (100 mm, P/B (100), 0.001–0.005 ohm cm) was purchased from University Wafer Inc. All experiments were conducted at room temperature. Ultrapure deionized (DI) water (18 MΩ) was used for all solution preparations and experiments.

2.2. Equipment and characterization

Scanning electron microscope (SEM) images were acquired using FEI Nova Nano SEM 430 microscope and QUANTA 400F Field Emission SEM. Prior to SEM analysis a thin Au/Pd alloy was deposited onto ITO and glass substrates. X-Ray diffraction (XRD) measurements were carried out on a Rigaku D Miniflex pc diffractometer with Cu Kα radiation ($\lambda = 1.54$ Å) operating at 30 kV. Varian Cary 100 Bio UV-Vis spectrometer with scan range of 190–1000 nm was used to monitor the formation of NPs. SERS measurements were performed using Horiba LABRAM Raman spectrometer operating with a He–Ne laser at 632.8 nm. A microscope with a 50× objective lens (numerical aperture 0.75) was used to focus the laser to a spot size around 1 μm^2. Samples were illuminated with 2 mW of power and the integration time was 20 s with five times accumulation.

2.3. Methods

2.3.1. Synthesis of spherical Au NPs. Three different sizes (4, 8 and 15 nm) of spherical Au NPs were synthesized as described in literature.[27] These NPs were used as seeds for the growth of branched NPs on surfaces. (i) *Synthesis of ca. 4 nm Au nanospheres*: first, 9.50 mL ultrapure water and 0.25 mL of 0.01 M $HAuCl_4 \cdot 3H_2O$ solution were mixed in a test tube. Then, 0.25 mL of 0.01 M sodium citrate solution was added to the mixture. Finally, 0.30 mL freshly prepared, ice-cold 0.1 M $NaBH_4$ solution was added and mixed rapidly for two minutes. The color of the solution was turned from orange to light-brown. The mixture was kept undisturbed at 27 °C in a water bath for three hours. (ii) *Synthesis of ca. 8 nm Au nanospheres*: here, *ca.* 4 nm NPs were used as seeds. Firstly, 45.0 mL of 0.08 M CTAB solution, 1.125 mL of 0.01 M $HAuCl_4 \cdot 3H_2O$ solution and 0.25 mL of 0.1 M freshly prepared AA solution were mixed in the given order by gentle inversion. Then, 5.0 mL of citrate stabilized seed solution (*ca.* 4 nm nanospheres) was added. The final mixture was stirred vigorously for 10 minutes. The solution was kept undisturbed at 27 °C in water bath for three hours. (iii) *Synthesis of ca. 15 nm Au nanospheres*: 8 nm spherical NPs prepared in the previous step were used as seeds in the synthesis of *ca.* 15 nm Au nanospheres. Similarly, 45.0 mL of 0.08 M CTAB, 1.125 mL of 0.01 M $HAuCl_4 \cdot 3H_2O$ and 0.25 mL of 0.1 M freshly prepared AA solutions were mixed in a test tube. Finally, 5.0 mL seed solution (*ca.* 8 nm spheres) was added. The final mixture was stirred for 10 minutes and kept undisturbed at 27 °C for three hours in a water bath.

2.3.2. Preparation of growth solution. The growth solution was previously reported for the synthesis of colloidal Au nanostars.[2] Here, the same solution was used for the synthesis of branched NPs on surfaces. It was prepared by mixing 4.75 mL of 0.1 M CTAB, 0.2 mL of 0.01 M $HAuCl_4$, 0.03 mL of 0.01 M $AgNO_3$ and 0.032 mL 0.1 M AA in the given order. The growth solution had a pH value of around 3. In order to find out the optimum pH value, strongly acidic (pH 1.45), neutral (pH 7.00) and basic (pH 10.00) solutions were prepared by adding either hydrochloric acid (HCl) or sodium hydroxide (NaOH) to the growth solution.

2.3.3. Preparation of surfaces for seed coating. First, substrates (Si-wafer and glass) were kept in 95–98% H_2SO_4 for about one hour. Then, substrates were thoroughly washed with ultrapure water. ITO was first washed with ultrapure water, then acetone and finally with ethanol. Finally, washed substrates were dried under nitrogen (N_2) gas. The functionalization of the surfaces with 3-aminopropyl-trimethoxysilane (APTMS) was performed by following a previously reported procedure.[19] Briefly, clean substrates were kept in 0.01% APTMS in toluene for 30 minutes. Then they were washed with ethanol and ultrapure water. Finally, substrates were dried under N_2 gas.

2.3.4. Growth of NPs on surfaces. First, APTMS covered substrates were incubated in the seed solution (spherical NPs) for 3 hours at room temperature. Later, substrates were removed from the seed solution, washed with ultrapure water several times and dried under N_2 gas. Finally, the synthesis of NPs was performed by placing seed-coated substrates into the previously prepared growth solution. The substrates were kept in these solutions at 27 °C overnight.

2.3.5. Preparation of SERS samples. R6G was used as a probe molecule and prepared at various concentrations for SERS studies. Next step of the SERS sample preparation involved immersing branched Au NPs grown on Si-wafer substrates in these solutions for two hours. Later, substrates were removed from R6G solution, washed with ultrapure water and dried under N_2 gas.

3. Results and discussion

A schematic illustrating the growth process of the branched Au NPs is provided in Fig. 1. The process has three main steps: (i) functionalization of the substrate surfaces, (ii) chemisorption of Au seeds on functionalized surfaces and (iii) growth of branched NPs on these surfaces.

In the first step, substrate surfaces were coated with APTMS, which functions as a linker between the substrate surface and Au seeds with spherical morphologies. The silanol end group of APTMS preferentially binds to the substrate surface, while amine end group interact with Au seeds. This allows anchoring of Au seeds onto the substrate surfaces.[26,28,29] Seed coated surfaces were washed carefully to remove excess Au seeds that were not

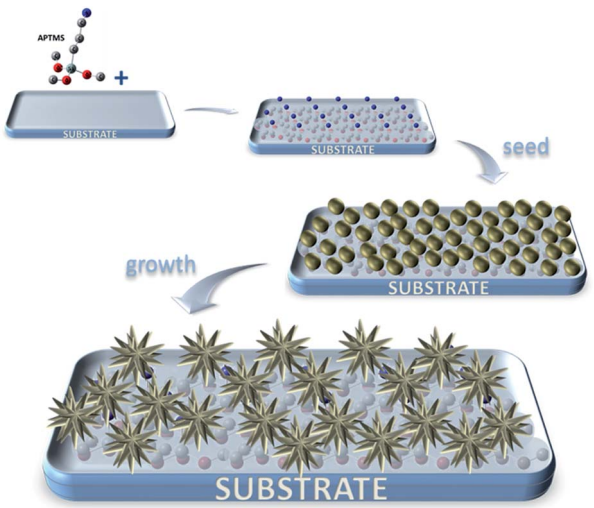

Fig. 1 Schematic representation of the growth of branched Au NPs on surfaces. Inset shows the structure of APTMS. Hydrogen atoms on APTMS are not shown for clarity.

adhered to the surface. Finally, the growth of branched Au NPs on APTMS coated substrate was achieved with "seed mediated growth" method by immersing substrates into the growth solution. The growth of branched NPs on glass and ITO substrates were monitored through the color change of the substrates. On the other hand, shiny Si-substrate surfaces turned matte upon NP growth. Absence of a color change in growth solution indicated that there was either no or very insignificant NP growth. This observation was also verified with the absence of any absorption band associated with Au NPs in the UV-Vis absorption spectra of the growth solution (Fig. S1, ESI†).

Syntheses of rod, wire and spherical nanostructures on surfaces have been reported previously using a similar experimental route.[19,26] In these studies, besides NPs in desired morphologies, significant amount of other morphologies were also formed. In our work, the reported procedures were modified and parameters such as the seed size and pH of the growth solution were optimized to synthesize the NPs in high yield and all with branched morphologies.

The investigation of optimum conditions revealed that the use of 8 nm Au nanospheres as seeds and growth solution with pH of *ca.* 3 yielded the desired branched nanostructures. Fig. 2 shows a SEM image of seed NPs (*ca.* 8 nm Au nanospheres) that are deposited on APTMS coated Si-substrate. The image verifies the successful attachment of seed NPs on the substrate surface.

Both high and low-magnification SEM images of branched Au NPs synthesized under optimum conditions on Si surfaces are provided in Fig. 3(a) and (b), respectively. The nanostructures have three dimensional morphologies with different numbers of sharp tips grown out of the NP core. SEM analysis revealed that all nanostructures synthesized at optimum conditions have branched morphology with average sizes (tip-to-tip distance) of *ca.* 450 ± 50 nm. Even though the synthesized nanostructures have a size variation of *ca.* 20%, no other particle morphologies were observed (Fig. 3).

The possible reasons for branching during NP growth have been suggested in various literature reports.[13,30–34] One reason might be a defect formation during reduction process of gold ions and poor binding of CTAB onto these defect sites. This lead to branching in the structure.[13,30–34] Another reason of branching is based on a process called under potential deposition.[35–37] Here, Ag^+ ions play a crucial role on anisotropic growth of NPs. The growth solution contain both $AuCl_4^-$ and Ag^+ ions (from $AgNO_3$). The higher reduction potential of $AuCl_4^-$ ions compared to the one of Ag^+ ions lead to preferential reduction of gold ions by ascorbic acid to form Au NPs. However, small amount of Ag^+ ions are also reduced and Ag(s) deposition occur on the growing NPs' surface. These Ag atoms are considered as nucleation sites, which promote branch formation in NP growth.[35–37]

SEM analyses show significant number of branched NPs was remained on the substrate surface even after multiple washing steps to remove unreacted reagents and/or non-bonded particles. In addition, providing a link between the substrate surface and Au NPs, APTMS is considered to play a crucial role on the growth of nanostructures on surfaces and on their morphologies.[19,28,29] It is suggested that amine groups of the APTMS on the substrate surface interact with Au(0) produced by the reduction of $AuCl_4^-$ in growth solution. Then, growing parts of Au nanostructures build new interactions with the neighboring amine groups on the functionalized surfaces. Thus, spontaneous growth of NPs and strong attachment to the surface can be achieved.[26]

Fig. 4 shows XRD pattern of branched Au NPs synthesized on Si-substrates under optimum reaction conditions. The pattern

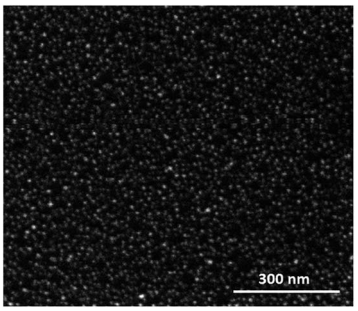

Fig. 2 SEM image of *ca.* 8 nm spherical Au NPs chemisorbed on APTMS coated Si-substrates.

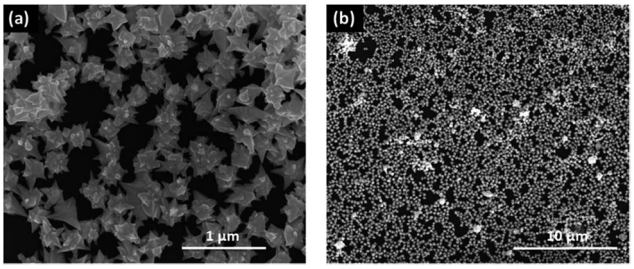

Fig. 3 SEM images (at different magnifications) of branched Au NPs on Si-substrates have shown with (a) 1 μm and (b) 10 μm scales.

exhibited diffraction peaks at 38.37°, 44.56° and 77.53° that were indexed to (111), (200) and (311) planes of face-centered cubic (fcc) Au, respectively (JCPDS card no. 65-2870).[38] A very low intensity peak for the (220) plane was observed at 64.51°. The other low intensity peaks observed at 34.47°, 40.05° and 69.40° were from the Si-substrate. The EDX analysis also verified the elemental identity of synthesized branched Au NPs (Fig. S2, ESI†). No impurities were detected within the resolution limits of XRD and EDX.

The synthesis of Au NPs on surfaces in desired yield and branched morphology was achieved by investigating the effect of reaction parameters (seed size and pH of the growth solution). This investigation yielded optimum parameters for the synthesis of targeted structures presented above. The details of this search are discussed in following sections.

3.1. Effect of seed size

Seed size has a determining role on the shape and size of the NPs produced in all synthesis methods using bottom-up approaches. Manipulation of this property provides the possibility of tuning the morphologies to obtain the desired nanostructures. In this study, three different sizes of spherical NPs were used as seeds to investigate their effect on the quality of the formed NPs. Other parameters such as reactant concentrations and pH (3.00) of the growth solution were kept constant in each set of the experiment to clearly observe the effect of seed size.

Fig. 5 shows the change in the size and shape of the synthesized nanostructures as a function of seed size. Comparison of these SEM images indicates that smaller particles were grown from the smaller seeds as expected. The nanostructures grown from the 4, 8 and 15 nm seeds have average sizes of *ca.* 290, 450 and 760 nm, respectively. The observed increase in synthesized NP size is most likely due to a decrease in the overall surface to volume ratio as the seed particle size increase. These cause an increase in the amount of gold ions per unit seed particle surface area since the gold ion concentration in the growth solution is constant. As a result of this, more gold ions are reduced on each seed particle surface leading to growing them into larger nanostructures. In general, growth of large NPs might also be associated with a secondary growth process called Ostwald ripening and defocusing.[39] In this process, particles with smaller size than the critical size dissolve and contribute to the growth of larger ones. Thus, larger particles grow into even larger structures. This is most likely the other possible reason for the formation of large structures as the seed size increase.

Besides the change in sizes of the synthesized NPs, differences in the yield of synthesized nanostructures were also observed upon the use of different seed sizes. Comparison of SEM images shows that yield of the branched NPs grown from 8 nm seeds (*ca.* 7 particle per μm^2) are higher with respect to the ones grown from 4 nm (*ca.* 1 particle per μm^2) and 15 nm (*ca.* 0.3 particle per μm^2) (Fig. 5). In addition, the variation in the size of the NPs grown from 8 nm seeds (between 409 nm and 511 nm) are much less than the ones grown from 4 or 15 nm seed particles (between 173 nm and 440 nm or between 533 nm and 933 nm, respectively) (Fig. 5d). The observed yield differences might be related with the size of seed particles and their surface area that is in contact with the APTMS on support. As the surface area of seed particles increase, the number of interaction sites on seed surface with the APTMS, which anchor them on surface, increase. On the other hand, if the seeds' size gets too large, they may become more susceptible to be washed out during purification process. The comparison of yields suggests that 8 nm seed particles have optimum properties (surface area and size) making them hold onto the surface better, resulting more branched NPs on the substrate surface.

3.2. Effect of pH

Literature is quite rich on examples where various types of NPs have been synthesized by simply changing pH of the growth solution.[30,40–42] The effect of pH is better understood when the

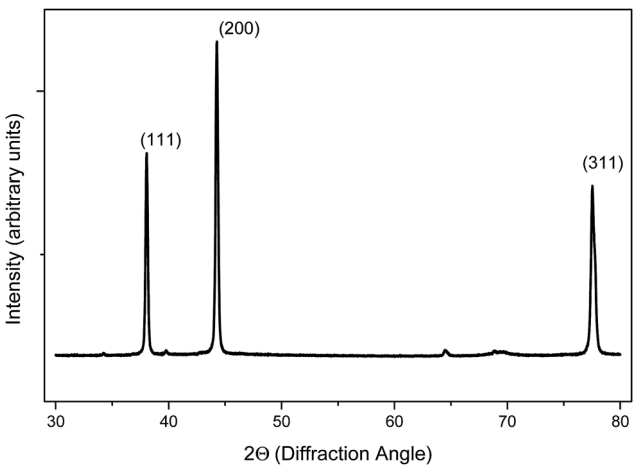

Fig. 4 XRD pattern of branched Au NPs on Si-substrates.

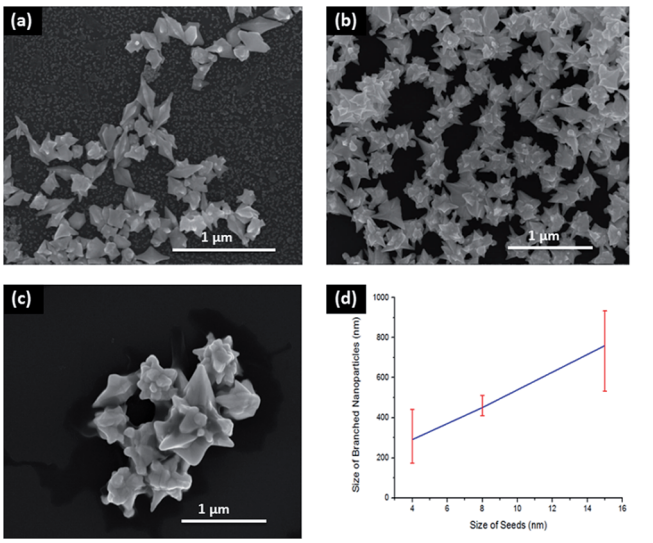

Fig. 5 SEM images of Au NPs grown on Si-substrates using spherical Au NPs as seeds with diameters; (a) 4.0, (b) 8.0, and (c) 15 nm. (d) The effect of seed size on the resulting nanoparticle diameter. Lines are for visual aid.

proposed ion exchange process and redox equilibrium taking place during NP growth are considered.[40] During this process, ion exchange between tetrachloroaurate ion ($AuCl_4^-$) and Br^- ions of CTAB to form $AuBr_4^-$ is believed to happen.[40] Then, this ion ($AuBr_4^-$) is reduced by ascorbic acid to form Au atoms according to the redox equilibrium given in eqn (1).

$$2AuBr_4^-(aq) + 3AH_2(aq) + 3H_2O(l) \rightleftarrows 2Au(s) + 3A(aq) + 6H^+(aq) + 8Br^-(aq) \quad (1)$$

here, AH_2 and A represent ascorbic and dehydroascorbic acid, respectively.

The addition of acid/base to the reaction media result in shifts in the equilibrium towards the reactants/products. This makes a significant change in dynamics (rate) of the proceeding reaction and provides some control over particle size and shape.[13,40–42] Therefore, it is crucial to have growth solution at an optimum pH value for the synthesis of desired NPs.

In this part of the study, pH of the growth solution was altered by adding strong acid (HCl) or base (NaOH). The effect of solution pH was investigated at four different pH values; that are strongly acidic (pH 1.45), acidic (pH 3.00), neutral (pH 7.00) and basic (pH 10.00). It should also be noted that, the results discussed here were from the sets of experiments that use 8 nm spherical seed NPs.

Fig. 6(a)–(d) shows SEM images of NPs obtained with pH values of 1.45, 3, 7 and 10, respectively. The comparison of these images reveals that the nanostructures do not have branched morphology and formed in a very low yield (*ca.* 1 particle per μm^2) in highly acidic media (pH 1.45) (Fig. 6a). The branching in the structure and the yield (*ca.* 7 particle per μm^2) increased significantly with an increase in solution pH (*ca.* 3.00) (Fig. 6b). Upon further increase in the solution pH to 7.00, the yield was still high (*ca.* 7 particle per μm^2) but the branching was not observed (Fig. 6c). Finally, formation of very low number of nanostructures was observed as the medium become basic (pH 10.00) (Fig. 6d).

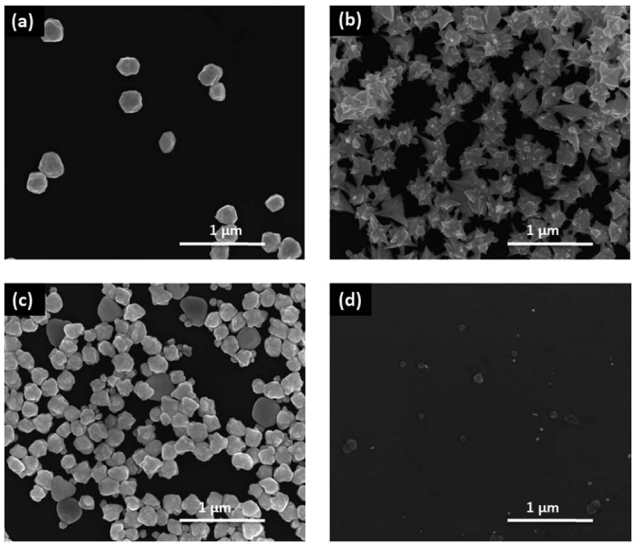

Fig. 6 SEM images of Au NPs synthesized on Si-substrates with (a) strongly acidic (pH 1.45), (b) acidic (pH 3.00), (c) neutral (pH 7.00), (d) basic (pH 10.00) growth solution. 8 nm seeds were used.

It appears that the dynamics of the growth process strongly depend on the solution pH. Formation of nanostructures without branched morphology at strongly acidic medium was most likely due to the suppressed reduction of gold ions with the increase in the number of H^+ ions in solution. A pH value of *ca.* 3 provided optimum conditions for the formation of desired nanostructures. On the other hand, the addition of NaOH to the growth solution promoted the reduction process and increased the formation of Au atoms in high rates in solution (eqn (1)). This speeds up the NP growth process and led to the formation of twin defects in crystal structure of the growing NPs.[13,30–34] Poor CTAB binding to defects is the most likely reason for growth anisotropy and branching of the NP as previously reported.[13,30–34] However, in this study, NaOH addition resulted in a decrease in the anisotropy and loss of branching in the structure. This is most likely because of the forced reduction of gold ions readily available in the growth solution by the added NaOH and formation of Au atoms, which then grow into NPs in the solution. Thus, the deposition of Au atoms that form branched NPs on the surface is hampered. As it was previously reported by Zhou *et al.*[30] Here too, a color change in the growth solution from colorless to red, the characteristic color of Au NPs in solution, was observed. Absorption band around 520 nm in UV-Vis absorption spectrum of this solution also verified the formation of Au NPs (Fig. S3, ESI†).

3.3. Synthesis of branched Au NPs on ITO and glass surfaces

The optimum seed size and growth media for the synthesis of branched NPs on Si-substrates were also utilized for the synthesis of these structures on ITO and glass surfaces. The results obtained from this investigation show that the same recipe can be applied to those surfaces as well for the potential future applications.

SEM images provided in Fig. 7(a)–(c) belong to Au NPs synthesized on Si, glass and ITO surfaces, respectively. Similar to the ones on Si-substrates, NPs on glass and ITO surfaces have branched structures with various numbers of tips grown out of the NP core. Even though the synthesized NPs have non-uniform morphologies with broad size distributions (between 350–500 nm), having all of the NPs with branched morphologies suggest that only one type of structure was synthesized on all three surfaces. In addition, since no major difference was observed within the shapes and sizes of NPs, it was concluded that the effect of surface on NP morphology was quite low. On the other hand, the results show surface type has an important effect on the obtained yield. The yield of NPs on ITO surface (*ca.* $1/\mu m^2$) was significantly lower than the ones on Si (*ca.* 7 particle per μm^2) and glass surfaces (*ca.* 3 particle per μm^2) (Fig. 7, S4 and S5, ESI†). There are two possible reasons for this observation. First one is the loose attachment of Au NPs on to APTMS coated ITO surfaces, leading to wash out of significant amount of NPs during purification. The second reason might be less effective binding of APTMS on ITO surface compared to that on glass and Si-substrates. Thus, lower number of Au seeds transfer to the

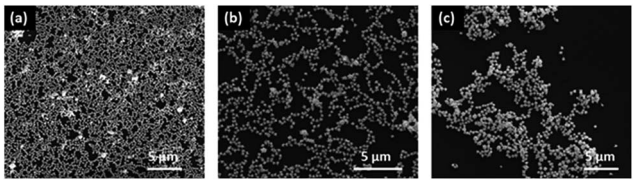

Fig. 7 SEM images of Au NPs synthesized on (a) Si-substrates, (b) glass, and (c) ITO surfaces. The synthesis was achieved through the use of 8 nm spherical NPs as seeds and growth solution with pH 3.00 in each set.

surface and less number of branched NP formation takes place. First reason is ruled out because Au NPs are expected to form strong bonds with the APTMS amine group and density of NPs on the surface depends on the number of APTMS molecules on the surface for binding. Therefore, possible weak interaction between APTMS and ITO surface is the most likely reason for observing less branched NP formation on ITO.

3.4. SERS studies

The SERS activity of branched Au NPs grown on Si-substrates was studied using R6G as a probe molecule. All of the vibrational modes of the R6G molecule were observed for all the batches of branched NPs on the Si-substrate tested (Fig. 8a).

The observed vibrational modes of the molecule agree well with those reported in the literature and assignments of the modes were based on these reports.[43] The molecules' signature modes associate with C–C–C ring in-plane bending at 618 cm^{-1}, out of plane bending at 779 cm^{-1}, aromatic C–C stretching at 1188, 1315, 1367, 1514, 1578 cm^{-1} and 1652 cm^{-1}, and C–H in plane bending vibration at 1130 cm^{-1} were clearly observed. The detection of relatively low intensity modes (below 600 cm^{-1}), which are most likely belong to Au–N stretching and ring bending, was also achieved with the use of synthesized NPs as SERS substrates. The comparison of the signal intensities in the measured SER spectrum of R6G on branched Au NPs to the Raman spectrum of the molecule reveals the significant enhancement of molecules' vibrational modes. The modes were not detectable in Raman spectrum of the probe molecule with 1 mM concentration, which are three orders of magnitude higher than the one on SERS substrates.

Enhancement factor (EF) calculation is quite challenging for nanostructures with branched Au NPs synthesized in this study as they do not have regular morphologies and well-defined surface areas. Therefore, we have estimated *rough, lower limit* EF by comparing the Raman and SERS signal intensity of mode at 1514 cm^{-1}. The following expression[12,44–47] was used to calculate EF:

$$\mathrm{EF} = (I_{\mathrm{SERS}}/I_{\mathrm{Raman}}) \times (N_{\mathrm{Raman}}/N_{\mathrm{SERS}}) \quad (2)$$

where I_{SERS} and I_{Raman} are the observed intensities of a vibrational mode in SERS and Raman, respectively. N_{Raman} and N_{SERS} are the number of analyte molecules excited under the laser spot in bulk sample and adsorbed on Au NPs, respectively. The I_{SERS} and I_{Raman} were measured for the R6G mode at 1514 cm^{-1}.

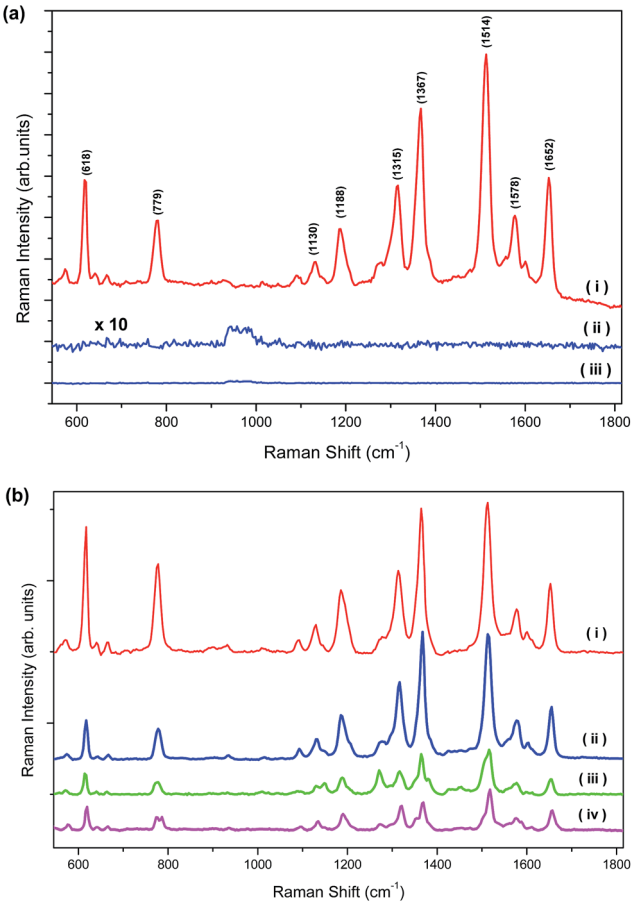

Fig. 8 (a) (i) SER spectrum of 1 μM R6G on branched Au NPs grown on Si-substrate. (ii) Raman spectrum of 1 mM R6G on Si-substrate (multiplied by 10). (iii) Raman spectrum of 1 mM R6G on Si substrate. (b) SER spectra of (i) 1 μM R6G, (ii) 0.1 μM R6G, (iii) 0.01 μM (10 nM) R6G and (iv) 0.001 μM (1 nM) R6G on branched Au NPs grown on Si-substrate.

The details of N_{Raman} and N_{SERS} calculations are given in ESI.† It is important to note that N_{SERS} calculations were done by assuming synthesized NPs having spherical morphologies with sizes *ca* 450 nm (average size of branched NPs) due to the aforementioned structural challenges and not well-defined surface areas of branched Au NPs. The calculations were performed for two different reported surface areas of R6G molecules in perpendicular (0.4 nm^2) and parallel (4 nm^2) orientations on NP surface.[48] Thus, the estimated EFs are *ca.* 2 $\times$ 10^8 and 2 $\times$ 10^9 for perpendicular and parallel orientations, respectively. EF calculations involve assumptions that all the analyte molecules added onto the SERS sample solution are adsorbed on NPs' surface and are making equal contribution to the measured SERS signal intensity. Therefore, the reported values are representing lower limits of EF and they are expected to be higher for branched Au NPs.

Evaluation of detection limits of NPs is another way to investigate their potential use of SERS substrates.[49–52] In this study, branched Au NPs demonstrated significant Raman enhancement between 0.01 μM and 1 μM R6G concentrations (Fig. 8b). The R6G modes were still clear at a R6G concentration

of 0.001 μM (1 nM) even though the signal intensity was significantly decreased. Detection of the molecule at this very low concentration with the use of branched Au NPs synthesized on Si-substrate makes the prepared system an attractive choice for further sensing applications.

4. Conclusions

In this study, the growth of branched Au NPs on APTMS coated Si-wafer, glass and ITO surfaces were achieved in high yield and all with single morphology. Parameters such as seed size and pH of the growth media were investigated. Among all the investigated seed sizes, 8 nm spherical Au NPs produced NPs in highest yield (*ca.* 7 particle per μm^2). In addition, an acidic growth medium with a pH of 3.00 was determined to be the optimum one for the synthesis of desired nanostructures. The synthesis of branched Au NPs was achieved on ITO and glass surfaces at these optimum conditions besides the Si-substrate. The use of different substrates did not make any significant changes in NP size and morphology. Besides the synthesis of branched Au NPs on surfaces with a facile route, potential use of these supported nanostructures as SERS substrates was demonstrated in this study. The Raman EFs for R6G molecule on branched Au NPs were estimated as 8 orders of magnitude or higher. Moreover, strong enhancements were observed for vibrational modes of the probe molecule even at very low concentrations (*e.g.* 1 nM). It is believed that NPs with special optical properties synthesized directly on different surfaces makes the fabricated systems very promising not only for sensing but also for photovoltaic and electronic device applications.

Acknowledgements

We acknowledge Assoc. Prof. Aysen Yilmaz (METU) for access to XRD instrument and Betul Cagla Arca (METU) for her help. We also acknowledge the support from METU-BAP Project: BAP-07-02-2014-007-168.

References

1 G. H. Jeong, Y. W. Lee, M. Kim and S. W. Han, *J. Colloid Interface Sci.*, 2009, **329**, 97–102.
2 E. Nalbant Esenturk and A. R. Hight Walker, *J. Raman Spectrosc.*, 2009, **40**, 86–91.
3 S. Yi, L. Sun, S. C. Lenaghan, Y. Wang, X. Chong, Z. Zhang and M. Zhang, *RSC Adv.*, 2013, **3**, 10139–10144.
4 S. Pedireddy, A. Li, M. Bosnan, I. Y. Phang, S. Li and X. Y. Ling, *J. Phys. Chem. C*, 2013, **117**, 16640–16649.
5 S. M. Novikov, A. Sánchez-Iglesias, M. K. Schmidt, A. Chuvilin, J. Aizpurua, M. Grzelczak and L. M. Liz-Marzán, *Part. Part. Syst. Charact.*, 2014, **31**, 77–80.
6 Q. Su, X. Ma, J. Dong, C. Jiang and W. Qian, *ACS Appl. Mater. Interfaces*, 2011, **3**, 1873–1879.
7 D. Kozanoglu, D. H. Apaydin, A. Cirpan and E. N. Esenturk, *Org. Electron.*, 2013, **14**, 1720–1727.
8 N. Li, P. Zhao and D. Astruc, *Angew. Chem., Int. Ed.*, 2014, **53**, 1756–1789.
9 B. Viswanathan. *Nano Materials*, Alpha Science International Ltd., Oxford, 2009, pp. 35–52.
10 S. K. Dondapati, T. K. Sau, C. Hrelescu, T. A. Klar, F. D. Stefani and J. Feldmann, *ACS Nano*, 2010, **4**, 6318–6322.
11 X. Huang, I. H. El-Sayed, W. Qian and M. A. El-Sayed, *J. Am. Chem. Soc.*, 2006, **128**, 2115–2120.
12 A. Li, Z. Baird, S. Bag, D. Sarkar, A. Prabhath, T. Pradeep and R. G. Cooks, *Angew. Chem.*, 2014, **126**, 12736–12739.
13 A. Guerrero-Martínez, S. Barbosa, I. Pastoriza-Santos and L. M. Liz-Marzán, *Curr. Opin. Colloid Interface Sci.*, 2011, **16**, 118–127.
14 A. J. Blanch, M. Döblinger and J. Rodríguez-Fernández, *Small*, 2015, **11**, 4550–4559.
15 S. Gilles, C. Kaulen, M. Pabst, U. Simon, A. Offenhäusser and D. Mayer, *Nanotechnology*, 2011, **22**, 295301–295308.
16 K. M. Hurst, N. Ansari, C. B. Roberts and W. R. Ashurst, *J. Microelectromech. Syst.*, 2011, **20**, 424–435.
17 R. G. Palgrave and I. P. Parkin, *J. Am. Chem. Soc.*, 2006, **128**, 1587–1597.
18 P. A. Pandey, G. R. Bell, J. P. Rourke, A. M. Sanchez, M. D. Elkin, B. J. Hickey and N. R. Wilson, *Small*, 2011, **7**, 3202–3210.
19 N. Taub, O. Krichevski and G. Markovich, *J. Phys. Chem. B*, 2003, **107**, 11579–11582.
20 C. J. Murphy, T. K. Sau, A. M. Gole, C. J. Orendorff, J. Gao, S. E. Hunyadi and T. Li, *J. Phys. Chem. B*, 2005, **109**, 13857–13870.
21 A. Sánchez, P. Díez, R. Villalonga, P. Martínez-Ruiz, M. Eguílaz, I. Fernández and J. M. Pingarrón, *Dalton Trans.*, 2013, **42**, 14309–14314.
22 N. R. Jana, L. Gearheart and C. J. Murphy, *Adv. Mater.*, 2001, **13**, 1389–1393.
23 W. Niu, L. Zhang and G. Xu, *Nanoscale*, 2013, **5**, 3172–3181.
24 S. Eustis and M. A. El-Sayed, *Chem. Soc. Rev.*, 2006, **35**, 209–217.
25 J. Liu, F. He, T. M. Gunn, D. Zhao and C. B. Roberts, *Langmuir*, 2009, **25**, 7116–7128.
26 M. Kambayashi, J. Zhang and M. Oyama, *Cryst. Growth Des.*, 2005, **5**, 81–84.
27 A. Gole and C. J. Murphy, *Chem. Mater.*, 2004, **16**, 3633–3640.
28 M. B. Haddada, J. Blanchard, S. Casale, J. M. Krafft, A. Vallee, C. Methivier and S. Boujday, *Gold Bull.*, 2013, **46**, 335–341.
29 K. C. Grabar, R. G. Freeman, M. B. Hommer and M. J. Natan, *Anal. Chem.*, 1995, **67**, 1217–1225.
30 J. Zhou, J. Zeng, J. Grant, H. Wu and Y. Xia, *Small*, 2011, **7**, 3308–3316.
31 M. Grzelczak, J. Peérez-Juste, P. Mulvaney and L. M. Liz-Marzan, *Chem. Soc. Rev.*, 2008, **37**, 1783–1791.
32 T. K. Sau and C. J. Murphy, *J. Am. Chem. Soc.*, 2004, **126**, 8648–8649.
33 E. Ye, M. D. Regulacio, S. Y. Zhang, X. J. Loh and M. Y. Han, *Chem. Soc. Rev.*, 2015, **44**, 6001–6017.
34 S. Chen, Z. L. Wang, J. Ballato, S. H. Foulger and D. L. Carroll, *J. Am. Chem. Soc.*, 2003, **125**, 16186–16187.

35 M. Liu and P. Guyot-Sionnest, *J. Phys. Chem. B*, 2005, **109**, 22192–22200.
36 C. G. Sanchez, M. G. Del Popolo and E. P. M. Leiva, *Surf. Sci.*, 1999, **421**, 59–72.
37 C. J. Orendorff and C. J. Murphy, *J. Phys. Chem. B*, 2006, **110**, 3990–3994.
38 C. Li, Y. Su, X. Lv, H. Xia and Y. Wang, *Sens. Actuators, B*, 2010, **149**, 427–431.
39 D. V. Talapin, A. L. Rogach, M. Haase and H. Weller, *J. Phys. Chem. B*, 2001, **105**, 12278–12285.
40 Y. N. Wang, W. T. Wei, C. W. Yang and M. H. Huang, *Langmuir*, 2013, **29**, 10491–10497.
41 F. Kim, K. Sohn, J. Wu and J. Huang, *J. Am. Chem. Soc.*, 2008, **130**, 14442–14443.
42 C. Zhu, H. C. Peng, J. Zeng, J. Liu, Z. Gu and Y. Xia, *J. Am. Chem. Soc.*, 2012, **134**, 20234–20237.
43 P. Hildebrandt and M. Stockburger, *J. Phys. Chem.*, 1984, **88**, 5935–5944.
44 E. Hao and G. Schatz, *J. Chem. Phys.*, 2004, **120**, 357–366.
45 D. A. Genov, A. K. Sarychev, V. M. Shalaev and A. Wei, *Nano Lett.*, 2004, **4**, 153–158.
46 P. Negri, R. J. Flaherty, O. O. Dada and Z. D. Schultz, *Chem. Commun.*, 2014, **50**, 2707–2710.
47 N. A. Cinel, S. Butun, G. Ertas and E. Ozbay, *Small*, 2013, **9**, 531–537.
48 A. Kudelski, *Chem. Phys. Lett.*, 2005, **414**, 271–275.
49 R. Lu, A. Konzelmann, F. Xu, Y. Gong, J. Liu, Q. Liu, M. Xin, R. Hui and J. Z. Wu, *Carbon*, 2015, **86**, 78–85.
50 J. Tang, H. Guo, M. Chen, J. Yang, D. Tsoukalas, B. Zhang, J. Liu, C. Xue and W. Zhang, *Sens. Actuators, B*, 2015, **218**, 145–151.
51 C. Wang, Y. Xu, H. Zhao, C. Gang, C. Lai, X. Liao and R. Wang, *Appl. Surf. Sci.*, 2015, **353**, 750–756.
52 R. Wang, Y. Xu, C. Wang, H. Zhao, R. Wang, X. Liao, L. Chen and G. Chen, *Appl. Surf. Sci.*, 2015, **349**, 805–810.